American Mineralogist, Volume 79, pages 606–614, 1994

Characterization of high-temperature phase transitions in single crystals of Steinbach tridymite

D. Cellai, M. A. Carpenter, B. Wruck, E.K.H. Salje
Department of Earth Sciences, University of Cambridge, Downing Street, Cambridge CB2 3EQ, U.K.

Abstract

Samples of tridymite from the Steinbach meteorite were examined by differential scanning calorimetry and X-ray single-crystal diffraction from room temperature to about 650 °C at 1 atm. The results confirm the existence of three phase transitions in the temperature range 350–475 °C, and a model involving O disorder is presented. In the temperature range 25–250 °C, the sequence and temperatures of phase transitions are strongly dependent on the thermal history. Crystals annealed in the stability field of the hexagonal phase develop an orthorhombic superstructure when subsequently held at temperatures between 100 and 154 °C. This superstructure has not been reported previously for Steinbach tridymite.

Introduction

Upon heating and cooling between room temperature and 700 °C, tridymite undergoes a series of displacive phase transitions. Many studies have been carried out on the thermal behavior of tridymite with a variety of techniques, including optical microscopy, single-crystal and powder X-ray diffraction, differential scanning calorimetry, differential thermal analysis, and infrared and nuclear magnetic resonance spectroscopy (complete references are given in recent papers by Smelik and Reeber, 1990; Graetsch and Flörke, 1991; De Dombal and Carpenter, 1993; Xiao et al., 1993), but a comprehensive model has not emerged. The number of phase transitions and their temperatures reported by different observers are often discordant, and it seems that the sequence of phase transitions is dependent on the starting material (terrestrial, meteoritic, synthetic, and industrial) and on the thermal history. The difficulty of characterizing a comprehensive sequence of phase transitions mainly arises from the lack of structure refinements at different temperatures. Even at room temperature several modifications exist, but the detailed crystal structures are known only for a few modifications. We have chosen to study the thermal behavior of natural tridymite from the Steinbach meteorite because its structure has been refined at different temperatures and also because, using the same sample, the sequence of transformations during heating is more reproducible.

The various crystal structures of tridymite have the same global topological features and can be described as sheets of six-membered rings of corner-sharing tetrahedra pointing alternatively up and down. They can be derived from the ideal hexagonal high-temperature modification (Gibbs, 1927) by rearranging the stacking of tetrahedral layers along the hexagonal **c** axis and distorting the six-membered rings within the layers. Some crystallographic data for the different phases from the literature are reported in Table 1.

Tridymite from the Steinbach meteorite is monoclinic at room temperature (phase MC), and its structure has been determined by Dollase and Baur (1976). According to Dollase (1967), this monoclinic structure transforms near 107 °C reversibly to a phase with a unit cell similar to that reported for hexagonal high tridymite (HP), but the reflections are accompanied by satellites in the pseudo-hexagonal **a*** direction, indicating a periodicity that varies continuously, from about 105 Å at 107 °C to about 65 Å at 180 °C (phase OS). Above this temperature, when the satellite reflections fade into the background, this phase transforms to orthorhombic high tridymite (phase OC). The ratio a/b of the OC phase is close to $\sqrt{3}$ so that the crystal symmetry is pseudohexagonal. According to Nukui et al. (1978), who studied a synthetic monoclinic tridymite (MC) from room temperature to 450 °C with X-ray precession techniques and optical methods, an orthorhombic superstructure (OP) with a cell $3 \times 1 \times 1$ compared with that of the orthorhombic OC phase is stable between MC and OS in the temperature range from 110 to 150 °C. The crystal structure of OP has been determined by Kihara (1977), who observed this phase in the temperature range from 100 to 160 °C. The OP phase has never been detected in the Steinbach tridymite. De Dombal and Carpenter (1993) reported two further phase transitions for Steinbach tridymite, at 350 and 465 °C. At 350 °C the orthorhombic OC structure becomes hexagonal, as shown by the merging of reflections excluding 00l (l = even), whereas the transition at 465 °C involves no change in crystal system and is characterized by a change in the gradient of the thermal expansion in the **c** direction.

According to some authors, the OC-HP transition is not a single transition as has been assumed in the past. Hoffmann and Laves (1964) and Czank et al. (reported

0003–004X/94/0708–0606$02.00

Table 1. Some crystallographic data for tridymite polymorphs

Phase	T (°C)	Space group	Unit cell (Å)	Ref.
MC*	25	Cc	a = 18.54 b = 5.00 c = 23.83 β = 105.7	a
OP	155	$P2_12_12_1$	a = 26.17 b = 4.99 c = 8.20	b
OS	107–180	incommensurate superstructure	a = 105–65	c
OS	150–190	metrically orthorhombic	a = 95–65 b = 5.02 c = 8.18	d
OC	220	$C222_1$	a = 8.74 b = 5.04 c = 8.24	c
HP	460	$P6_3/mmc$	a = 5.05 c = 8.27	e

Note: the unit-cell parameters refer to the temperature reported in the second column; a = Dollase and Baur (1976), b = Kihara (1977), c = Dollase (1967), d = Nukui et al. (1978), e = Kihara (1978).

* The Hoffmann (1967) setting is a = 18.5, b = 5.0, c = 25.8 Å; β = 118°.

in Flörke, 1967) observed diffuse reflections in the hexagonal phase that should not be present in the $P6_3/mmc$ space group. Nukui et al. (1978) observed diffuse reflections violating c-glide absences ($\bar{h}2hl$, l = odd) and persisting up to 450 °C, 70 °C above the orthorhombic-hexagonal transition. NMR and infrared spectroscopy (Xiao et al., 1993, and De Dombal and Carpenter, 1993) showed a structural effect between 340–490 °C and 360–460 °C, respectively, which suggests the existence of an intermediate phase between OC and HP.

The purpose of the present paper is to clarify the nature of these high-temperature transitions that seem to occur in all tridymite. The results of X-ray single-crystal diffraction and differential scanning calorimetry studies are reported. Evidence from infrared spectroscopy will be reported in another paper.

Experimental details

Sample description

The tridymite sample, from the Steinbach meteorite, was provided by the British National History Museum (no. 33540). Steinbach tridymite is a very pure natural tridymite. Wet-chemical analysis (Grant, 1967) gives an SiO_2 content of 99.5 wt%. Major impurities are Al, Na, and Fe (Grant 1967; Reid et al., 1974; Dollase, 1967). When viewed under the optical microscope with crossed nicols, the crystals were usually twinned. The twinning involves individuals related by sixfold rotation around the morphologic **c** axis (normal to the hexagonal platelets). Similar twinning has been described previously (Dollase and Baur, 1976; Hoffmann, 1967; Tagai et al., 1977). Several dozen grains were selected that appeared to be untwinned optically. Most of these fragments were then discarded after a first X-ray test with oscillation photographs, but two crystals (0.5 × 1 × 1 mm size) that seemed to be untwinned from the oscillation photographs were used for further X-ray investigations.

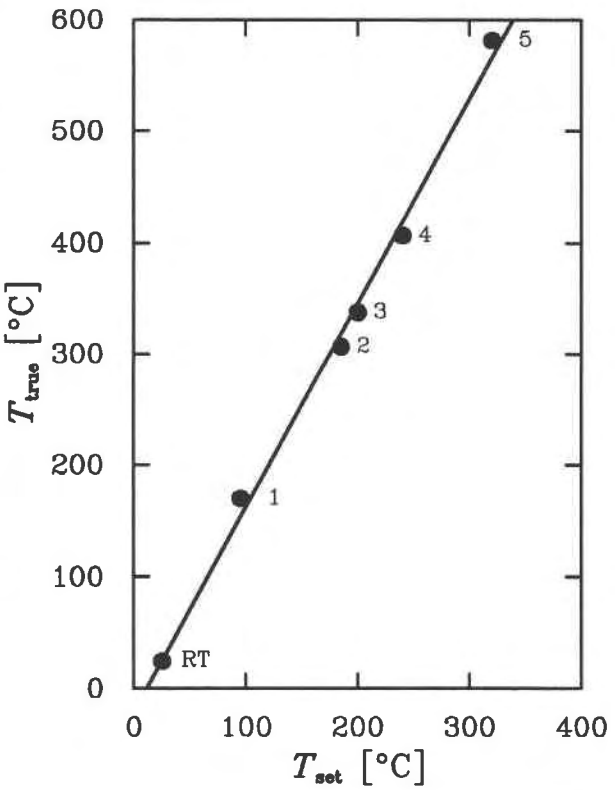

Fig. 1. Plot of the temperature calibration for the X-ray diffractometer furnace. T_{set} represents the thermocouple temperature, and T_{true} the melting point of known standards; 1 = H_3BO_3, 2 = $NaNO_3$, 3 = KNO_3, 4 = $K_2Cr_2O_7$, 5 = KIO_4.

High-temperature single-crystal X-ray methods

X-ray experiments were carried out using a Philips PW1100 four-circle diffractometer with graphite monochromatized Mo$K\alpha$ radiation and a STOE precession camera with unfiltered Mo radiation. In both cases, the crystals were heated by an electrical resistance furnace. In the four-circle diffractometer, the thermocouple was situated about 5 mm from the crystal. This led to a significant difference between the true temperature of the sample and that at the measuring thermocouple. Therefore a calibration experiment was carried out. The melting points of five samples were measured for temperature calibration. The results are shown in Figure 1, and a least-squares linear fit to the data gave T_{true} = 1.83 T_{set} − 21 °C, with a precision of ±15 °C.

In an initial series of experiments, intensity measurements of the 041 reflection in the orthorhombic setting, which corresponds to $\bar{2}41$ in the hexagonal system and is systematically absent in the space group $P6_3/mmc$, were collected from room temperature up to 630 °C in steps of ca. 50 °C. The same crystal was then used for a further heating experiment from room temperature to 630 °C in

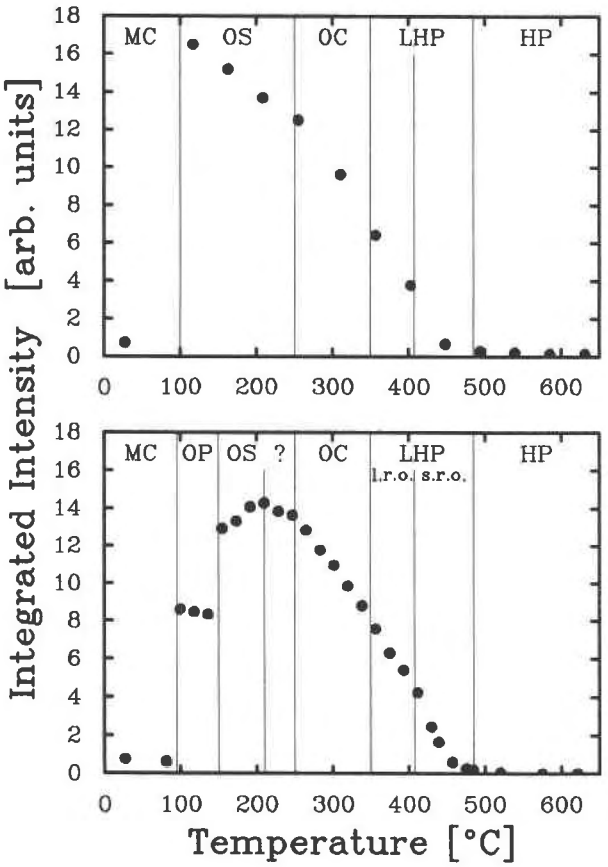

Fig. 2 Change of the integrated intensities (arbitrary scale) with the temperature of the 041 reflection (orthorhombic setting), which is $\bar{2}41$ in the hexagonal setting, for the first heating experiment (Fig. 2, **top**) and after annealing in the stability field of the hexagonal phase (Fig. 2, **bottom**). The positions of the phase boundaries interpreted from data in the literature and from the present experimental study are shown as vertical lines.

steps of ca. 20 °C. After the first heating experiments, the crystal seemed to be twinned. Integrated intensities were measured using an ω scan across the diffraction peak with a scan width of 2° and a speed of 0.005°/s. Background intensities were measured on either side of the peak, and a linear interpolation was used to calculate the total background. A measurement of the peak profile was taken in ω and $\omega/2\theta$ scans to check whether the peak became diffuse with increasing temperature. A least-squares fit was performed using a Gaussian diffraction profile for the 041 reflection to calculate the peak width. Cell dimensions were determined by least-squares fitting of 24 reflection positions measured on the diffractometer.

Precession photographs were taken for the **c*-b*** plane in the orthorhombic setting, which corresponds to **c***-$[\bar{h}2h0]$* in the hexagonal setting, to monitor the behavior of the 041 reflection as a function of temperature. The exposure times were 2 weeks for experiments below 350 °C and 6–8 weeks for those above 350 °C.

Differential scanning calorimetry

Clean grains were separated by hand, yielding 22.676 mg of sample. The grains had long diameters between 0.2 and 0.5 mm and were not subjected to any grinding. All samples were weighed to a precision of 0.002 mg by means of a Mettler M5 balance. The heat capacities were measured using a Perkin-Elmer DSC7 differential scanning calorimeter. The measurements were made at a heating rate of 10 °C/min. Temperature calibrations were carried out by measuring the melting temperatures of In, Sn, Pb, and Zn at 156.60, 231.88, 327.45, and 419.47 °C, respectively, and the transition temperatures of K_2SO_4 and K_2CrO_4 at 585 and 665 °C. The specific heats were determined using sapphire as a C_P reference standard. Reference values were taken from Ditmars and Douglas (1971). Several measurements were made for overlapping temperature intervals of 60–70 °C between 260 and 640 °C, except for the first measurement carried out in the interval from 80 to 300 °C. For each interval, five sets of heat capacities were measured, alternating the tridymite sample, the sapphire standard, and the empty pan, and the average C_P value was determined. After several cycles of heating and cooling, a DSC scan was made from 80 and 300 °C to determine the influence of high-temperature annealing on the low-temperature phase transitions.

Results

Single-crystal X-ray diffraction

The temperature evolution of the integrated intensity of the 041 reflection (in the orthorhombic setting, which is the $\bar{2}41$ reflection in the hexagonal setting) for the first heating experiment is shown in Figure 2 (top). The reflection is very weak at room temperature. At 110 °C the intensity increased by a factor of 20, corresponding to the transition from the MC to the OS phase. On further heating, the intensity decreased continuously, showing a change of slope at about 250 °C, and disappeared at 475 ± 15 °C. The second heating experiment (Fig. 2, bottom) gave different results at temperatures below 250 °C. Six features can be identified between room temperature and 630 °C (Fig. 2, bottom), probably corresponding to phase transitions. The first one, at 100 ± 15 °C, is characterized by a sudden increase of the intensity and is due to the MC to OP transition. The presence of the OP phase, which did not appear in the first heating experiment, has been verified by detecting the presence of the 810 superstructure reflection. This reflection is sharp and vanishes into the background at 150 °C (Fig. 3), where a further strong increase of the 041 reflection occurs under heating (Fig. 2, bottom). During heating from 150 to 210 °C, the intensity of the 041 reflection increases and then starts to decrease continuously. Another change in slope occurs at 250 ± 15 °C, corresponding to a fourth transition. All these phase transitions can be correlated with the DSC measurements described later. With regard to the transition at 250 °C, many authors (Mosesman and Pitzer, 1941; Shahid and Glasser, 1970; Flörke and Müller-Von-

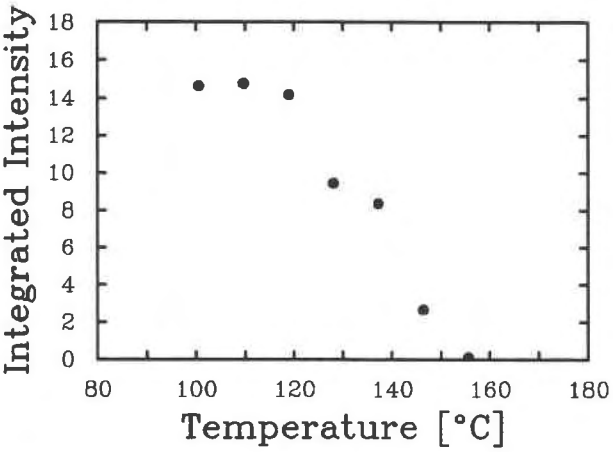

Fig. 3. Integrated intensities (arbitrary scale) of the 810 superstructure reflection of the OP phase. The decrease to zero is assumed to mark the transition OP → OS.

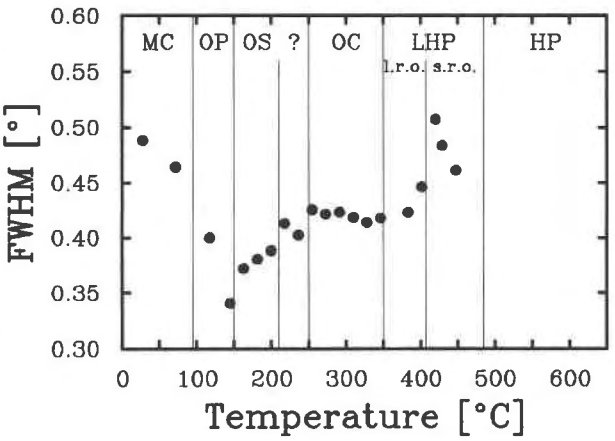

Fig. 4. Plot of the peak width (full width at half maximum) for the 041 reflection as a function of temperature. The peak profile has been measured using an ω scan.

moos, 1971; Thompson and Wennemer, 1979; Wennemer and Thompson, 1984) proposed that this transition in tridymite is actually the low-high inversion of cristobalite, which may be intimately interlayered with tridymite. However, our X-ray observations show it to be a real effect in Steinbach tridymite as we did not find evidence for the presence of cristobalite in any of the X-ray diffraction patterns.

Using linear extrapolation, the intensity of the 041 reflection would disappear at 475 ± 15 °C. The decrease of the intensity is not a linear function of temperature, however, and a further change in slope is observed at about 400 °C. The orthorhombic-hexagonal transition, which has been reported for Steinbach tridymite at 350 ± 10 °C by De Dombal and Carpenter (1993) does not show up either in the intensity data (Fig. 2) or in the DSC data. The transition can be identified easily in the X-ray powder traces by the coalescence of the split reflections at 350 ± 10 °C, however. This confirms the existence of the transition without detectable changes of the intensity of the 041 reflection.

Precession photographs recorded at different temperatures for the **b*-c*** plane (orthorhombic setting) showed a similar behavior of the intensity of the 041 reflection to that observed on the four-circle diffractometer.

The peak profile of the 041 reflection was measured at different temperatures on the four-circle diffractometer during the second experiment, and its half width as a function of temperature is shown in Figure 4. In the MC phase, the 041 reflection (which corresponds to 240 in the monoclinic *Cc* structure using the setting of Hoffmann) is very weak and broad. When the intensity increases substantially at ~100 °C, the peak becomes sharper. At about 150 °C, an increase of the peak width is then observed. In the temperature range of the OS phase, the peak width increases. The third change occurs at about 250 °C where the peak width becomes almost constant. At 400 °C the peak becomes very broad, and this change correlates with the change in slope of the intensity at about 400 °C in Figure 2 (bottom). Above 440 °C the peak is very weak, and we did not fit a peak profile for determining the half width.

The unit-cell dimensions measured on heating for the second experiment are shown in Figure 5. An abrupt change corresponding to the transition between the monoclinic form and the orthorhombic OP form is clearly seen in the *a, b,* and *c* parameters. A second rapid change in the *b* parameter occurs at 150 °C and is due to the OP-OS transition. The *c* parameter shows a marked reduction in the thermal expansion at 475 °C, corresponding to the disappearance of the 041 reflection. Similar behavior of the *c* and *a* lattice parameters has been reported in Kihara (1978), Graetsch and Flörke (1991), and De Dombal and Carpenter (1993).

Differential scanning calorimetry

The heat flows in the first heating experiment from 80 to 300 °C show two peaks at 105 and 112 °C (Fig. 6a). According to Dollase (1967), in this temperature range the transition MC to OS occurs, but the presence of the double peak indicates that probably two phase transitions occur. Unfortunately, up to now no structure refinement has been done between these two temperatures. Small effects on heating can be seen at 143, 160, 165, 195, and 225 °C in Figure 6b. In the second heating scan, the temperatures of the two lowest temperature peaks were about 5 °C lower than in the first (Fig. 6c), and a change in C_P was found for the transition near 195 and 225 °C (Fig. 6d). The resulting C_P curve then remained reproducible as checked in three subsequent experiments. The C_P anomaly at 143 °C can be seen more clearly in Figure 7.

The change in transition temperature after heating was also reported by Wennemer and Thompson (1984) and by Cohen and Klement (1980). After repeated thermal cycling in the stability field of the hexagonal phase, the temperature range from 80 to 300 °C was reinvestigated.

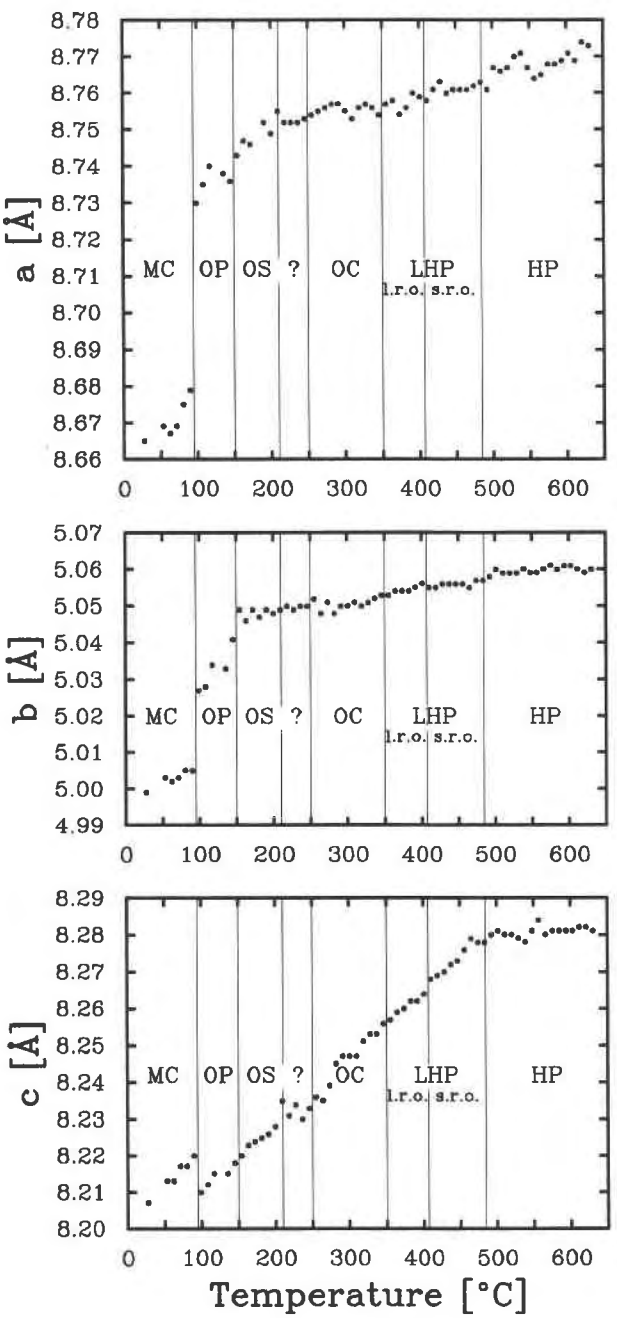

Fig. 5. Thermal expansion behavior of Steinbach tridymite after annealing the crystal at high temperature (in the stability field of the hexagonal phase). The lattice parameters (*a, b, c*) correspond to the cell of the OC phase.

A change in the transition behavior was observed (Fig. 6e, 6f), and a new peak appeared at 154 °C. The new phase transition is due to the change from OP to OS as shown in the X-ray experiments (Fig. 2, bottom, Fig. 3). It seems that annealing in the stability field of the hexagonal phase or cooling and quenching conditions can create structural defects that prevent a reappearance of the incommensurate OS phase directly from the MC structure and that result in the development of an intermediate commensurate OP phase.

Now let us analyze the total transition enthalpies. The latent heat of the MC-OS transition in the first heating experiment of the virgin sample is 6.43 J/g (Fig. 6a). After annealing, this transition does not occur directly but in two steps by means of an intermediate phase: MC → OP → OS. The transition enthalpies are now 1.88 J/g for the transition at 154 °C and 4.55 J/g for the transition between 95 and 115 °C. The most interesting result is that the sum of these two transition enthalpies after annealing is the same as the transition enthalpy for MC → OS before annealing.

At T_c = 407 °C, a sharp step occurs in the specific heat data, indicating a second-order phase transition (Fig. 8). A broad peak near 400 °C was also observed by De Dombal and Carpenter (1993), but their heat capacity measurements were performed on a powdered sample that had been ground by mortar and pestle. Cohen and Klement (1980) reported that the width of the transition depends on the sample size, which explains why the transition is spread out in the experiment by De Dombal and Carpenter (1993). The transition at 350 °C, seen, for example, in the splitting of the X-ray powder lines (De Dombal and Carpenter, 1993), shows virtually no detectable anomaly in C_P. For temperatures above T_c, we found a small tail in the excess specific heat that vanishes near 475 °C. This is the same temperature at which both a change in the temperature slope of the *c* lattice parameter (Fig. 5) and the disappearance of the intensity of the 041 reflection (Fig. 2) occur.

The excess specific heat near the 407 °C anomaly can now be analyzed. The excess specific heat, ΔC_P, is defined as the difference between the specific heat of the low-temperature phase and the extrapolated specific heat of the high-temperature phase. For the determination of the extrapolated specific heat, C_P°, an empirical temperature dependence of the form $C_P^\circ = c_0 + c_1 T + c_2 T^2$ was used. The excess specific heat, ΔC_P, in Landau theory for a second-order transition has the temperature dependence

$$\Delta C_P = \frac{a^2}{2b} T \qquad \text{for } T < T_c$$

$$\Delta C_P = 0 \qquad \text{for } T > T_c$$

where *a* and *b* are the coefficients of the Landau potential,

$$G = a/2\,(T - T_c)Q^2 + b/4\,Q^4.$$

The Landau potential is written here for a single order parameter *Q*, ignoring possible coupling with the transitions at 350 and 475 °C. In the two temperature ranges, $T < 407$ and $T > 507$ °C, the experimental C_P values were fitted numerically to the function $C_P = C_P^\circ + \Delta C_P$. The term ΔC_P gives no contribution for the high-temperature interval, $T > 507$ °C. The calculated values of the specific heat were compared with the experimentally ob-

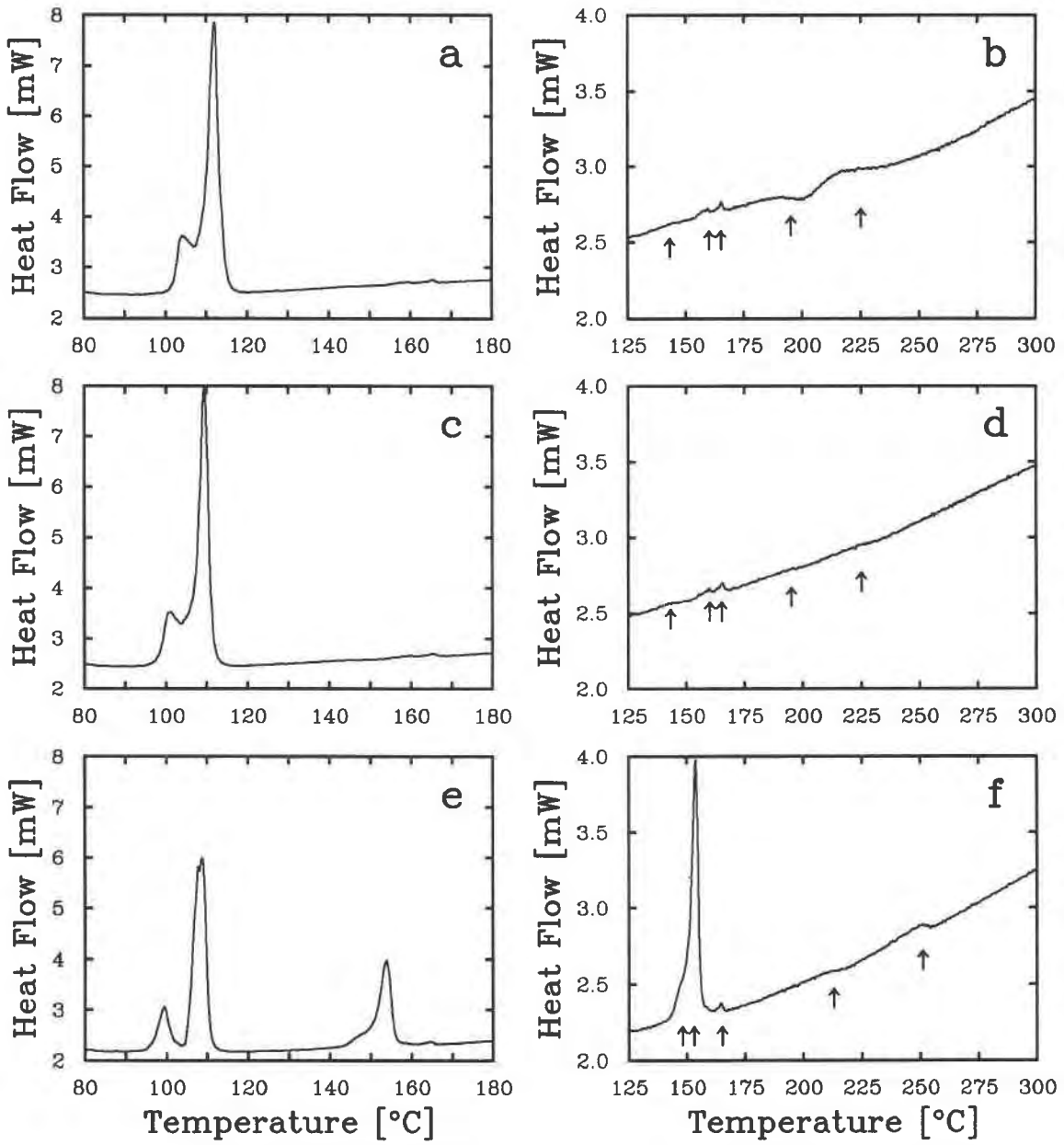

Fig. 6. Tracing of DSC scans for tridymite between 80 and 300 °C; *a* and *b* represent the first heating experiment; *c* and *d* represent the subsequent heating experiment; *e* and *f* represent a heating experiment after the tridymite crystals had been annealed at high temperature (in the stability field of the hexagonal phase). The arrows represent anomalies in C_P.

served values in an objective function calculating the mean relative error:

$$\eta = \frac{1}{N} \Sigma \left| \frac{y^{obs} - y^{calc}}{y^{obs}} \right|.$$

This function was minimized with respect to the parameters c_0, c_1, c_2, and $a^2/(2b)$, using a Nelder-Mead downhill simplex method (Press et al., 1986). The strategy in trying to find the global minimum has been described in Wruck et al. (1991). The final values for the parameters are

$$c_0 = 43.83 \text{ J/(mol·K)}$$

$$c_1 = 3.535 \cdot 10^{-2} \text{ J/(mol·K}^2\text{)}$$

$$c_2 = -7.967 \cdot 10^{-6} \text{ J/(mol·K}^3\text{)}$$

$$\frac{a^2}{2b} = 1.40 \cdot 10^{-3} \text{ J/(mol·K}^2\text{)}$$

$$T_c = 679.5 \text{ K}.$$

The mean relative error η for this fit is <0.087%. The

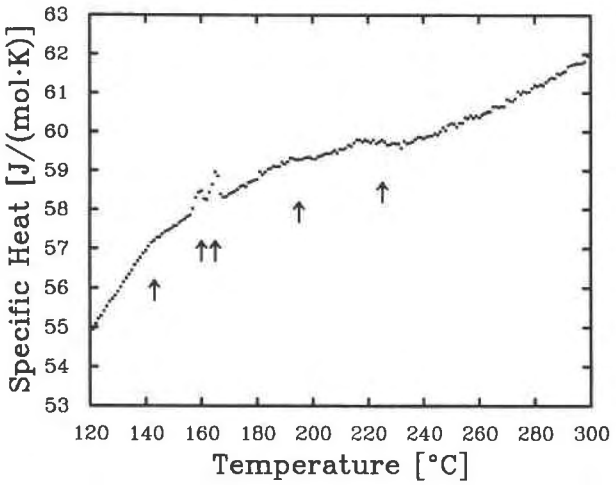

Fig. 7. Specific heat as a function of temperature in the temperature range 120–300 °C. The arrows point to the anomalies in C_P.

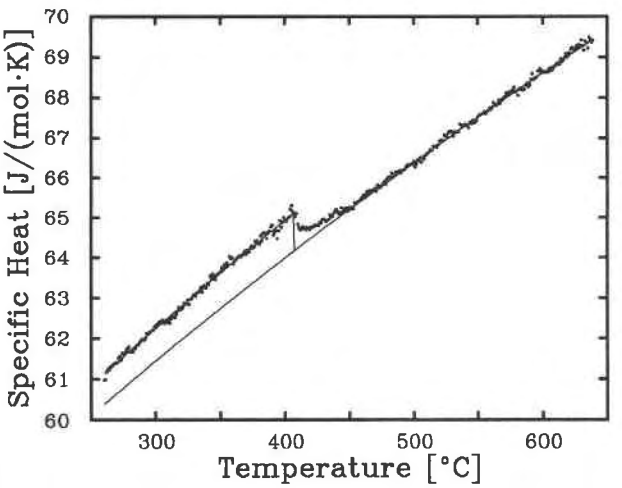

Fig. 8. Specific heat as a function of temperature in the temperature range 260–640 °C showing a sharp step at T_c = 407 °C. A small tail in the excess specific is present above T_c and vanishes at 475 °C.

resulting curve for C_P° is shown in Figure 8. Figure 9 shows the excess specific heat. The vanishing of the tail in ΔC_P at 475 °C can be seen clearly.

The excess entropy resulting from the transition, ΔS, was calculated from the ΔC_P data using the relationship

$$-\Delta S\,(T) = \int_T^{T_c} \frac{\Delta C_P}{T}\,dT.$$

Since we observed a tail in the excess specific heat above T_c, we chose for the upper limit of the integral not T_c but 639 °C, the temperature of the last data point. This procedure does not change the relative temperature dependence of ΔS below T_c but allows the estimation of the entropic effect at $T > T_c$. The values of ΔS as a function of temperature are shown in Figure 10. As the values of ΔC_P vary statistically around zero at $T > 475$ °C (Fig. 9), contributions to the integral cancel with $\Delta S = 0$ (Fig. 10). For temperatures less than T_c, the excess entropy shows a linear temperature dependence. The slope of $\Delta S\,(T)$ at $T < T_c$ was used to determine the coefficients of the Landau potential assuming a single order parameter. Scaling the order parameter to $Q = 1$ at $T = 0$ K leads to a = 1.903 J/(mol·K), and b = 1293 J/mol. Comparison between the experimental data and the simple model shows that a Landau potential with one order parameter does not describe the details of the transition, although it gives an approximation for the differences in the thermodynamic quantities between the high-temperature (HP) and low-temperature (LHP) hexagonal phases.

Discussion

Anomalies in the heat capacity data between 80 and 640 °C correlate with changes in the intensity of the 041 reflection. This reflection, which is $\bar{2}41$ in the hexagonal setting, is absent in the space group $P6_3/mmc$ because of the presence of the c glide. The disappearance of the reflection at 475 ± 15 °C is accompanied by a rapid decrease of the thermal expansion along **c** and by the vanishing of the tail in the excess specific heat. Above 475 °C the tridymite structure has achieved a fully expanded state, showing low thermal expansion in the **a** and **c** directions, and its space group is $P6_3/mmc$ (HP). Structure refinements of the HP phase (Kihara, 1978) show that there is a large displacement amplitude normal to the Si-O-Si bond, indicating a strong positional disorder. Ambiguity remains for the O positions because the difference-Fourier map did not clearly show whether the O atoms are located on discrete positions (probably six) on the circumference of the circles perpendicular to the Si-Si axis or whether they move around the circumference without fixed positions. In the temperature range 350–475 °C, the symmetry of tridymite is hexagonal on a macroscopic length scale (because of the merging of reflections excluding $00l$, l = even), but its space group cannot be $P6_3/mmc$ because of the presence of reflections violating the c-glide (e.g., $\bar{2}41$). At 407 °C a transition that is clearly second order in character, from the specific heat data, correlates with the sudden increase in the width of the 041 reflection.

A model involving O disorder may be proposed to explain all this experimental evidence for the high temperature transitions. In the OC phase (below 350 °C) O disorder is still present, and the density distribution of the O atoms (Kihara et al., 1986) shows that the atoms do not occupy equally all the six positions located around a ring. Above 350 °C the O atoms occupy statistically all the six positions without overcoming the central barrier (i.e., without passing through the center of the circle). The consequence is that the crystal does not have the inversion center, and the average structure is $P6_322$ (LHP). At 407 °C the O atoms begin to overcome the central barrier (flipping movements), and the crystal becomes nonpiezoelectric. Because the flipping probably does not occur

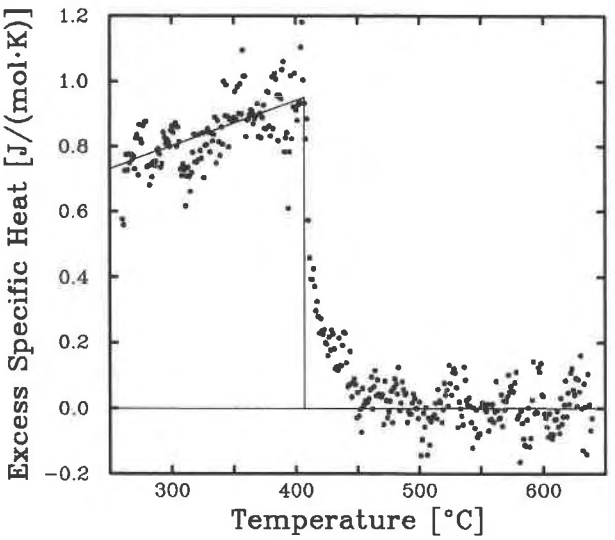

Fig. 9. Excess specific heat (ΔC_P) as a function of temperature showing the transition at 407 °C and the vanishing of the tail in ΔC_P at 475 °C.

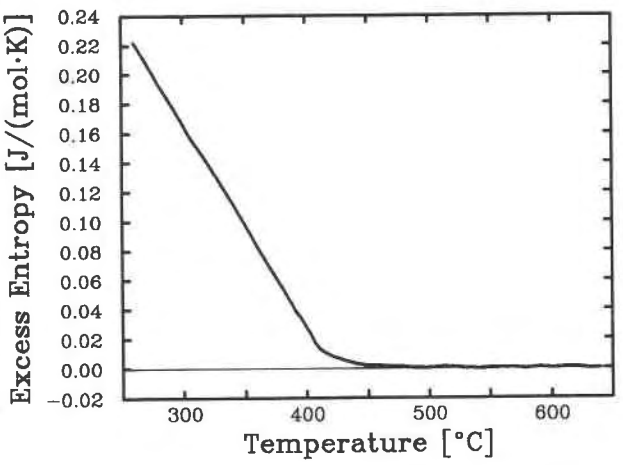

Fig. 10. Excess entropy (ΔS) resulting from the transition at 407 °C. The excess entropy goes to zero at 475 °C and has a linear temperature dependence below T_c = 407 °C.

with a high enough probability, microdomains of the LHP phase are still present up to 475 °C. Above 475 °C (HP) the central barrier can be overcome so that the O atoms can move readily both around the rings and across the centers of the rings. Thus, on cooling, the initial change from the HP structure is the development of microdomains of LHP without long-range correlations. The reflections violating the *c*-glide are diffuse at this stage, and the tail in ΔC_P indicates the magnitudes of the energies involved. At 407 °C the LHP domains become large, as indicated by sharpening of the glide-violating reflections. There is a substantial change in energy associated with this increase in correlation length, as shown by the discrete second-order step in C_P. The subsequent transition LHP → OC involves some ordering of the O atoms around the ring, but the energy associated with this is very small.

The model is consistent with the ^{29}Si MAS NMR spectra of tridymite (Xiao et al., 1993). In the temperature range 340–490 °C, the positions of the NMR peaks do not change, implying that the average Si-O-Si bond angle remains the same. The movement of the O atoms around the rings or across the centers of these rings gives the same average Si-O-Si bond angle.

The transition behavior below 250 °C is strongly dependent on the thermal history of the tridymite crystal. Crystals that are heated to 300 °C have the MC-OS transition 5 °C lower than the unheated crystals. A change in the intensity of the C_P anomalies at 195 and 225 °C also occurs. The transition MC → OS requires a large amount of energy because of the change in the stacking sequence and in the shape of the rings within the layers. Small C_P anomalies in the temperature range 143–225 °C may reflect changes of the satellite reflections of the OS phase. According to Nukui et al. (1978), the satellite reflections are influenced by the change of the Si-O-Si bond angles along the [100] direction of the OS phase.

Many temperatures for the OS-OC transition have been reported. Dollase (1967) briefly mentioned the transition at 180 °C at which satellite reflections in X-ray procession photographs fade into background. Nukui et al. (1978) reported the transition at 190 °C with the satellites changing into diffuse streaks. From NMR results (Xiao et al., 1993), the temperature of the transition is marked by the disappearance of the shoulder of the peak at about 210 °C. From our DSC measurements, the OS-OC transition is at 225 °C for the unheated and heated (to 300 °C) crystals of tridymite.

When the tridymite crystals are heated at high temperature (in the stability field of the hexagonal phase), a new phase (OP) is formed between MC and OS, and the OS-OC transition is shifted to 250 °C. In this case the satellite reflections of the OS phase lock into a commensurate position, producing the OP phase in the temperature range 100–154 °C. This new sequence of phase transitions MC → OP → OS is the same as that found in synthetic tridymite. Presumably the effect of high-temperature annealing is to change the character or distribution of defects.

Acknowledgments

We would like to thank Kuniaki Kihara and an anonymous referee for their helpful reviews. D.C. acknowledges the receipt of an EEC (Human Capital) grant and thanks the Ministero della Pubblica Istruzione in Italy (MPI 40%).

References cited

Cohen, L.H., and Klement, W., Jr. (1980) Tridymite: Effect of hydrostatic pressure to 6 kbar on temperatures of two rapidly reversible transitions. Contributions to Mineralogy and Petrology, 71, 401–405.

De Dombal, R.F., and Carpenter, M.A. (1993) High-temperature phase transitions in Steinbach tridymite. European Journal of Mineralogy, 5, 607–622.

Ditmars, D.A., and Douglas, T.B. (1971) Measurement of the relative

enthalpy of pure α-Al_2O_3 (NBS heat capacity and enthalpy standard reference material no. 720) from 273 to 1173 K. Journal Research NBS, 75A (5), 401–420.

Dollase, W.A. (1967) The crystal structure at 220 °C of orthorhombic high tridymite from the Steinbach meteorite. Acta Crystallographica, 23, 617–623.

Dollase, W.A., and Baur, W.H. (1976) The superstructure of meteoritic low tridymite solved by computer simulation. American Mineralogist, 61, 971–978.

Flörke, O.W. (1967) Die Modifikationen von SiO_2. Fortschritte der Mineralogie, 44, 181–230.

Flörke, O.W., and Müller-Vonmoos, M. (1971) Displazive Tief-Hoch-Umwandlung von Tridymite. Zeitschrift für Kristallographie, 133, 193–202.

Gibbs, R.E. (1927) The polymorphism of silicon dioxide and the structure of tridymite. Proceedings of the Royal Society of London, A113, 351–368.

Graetsch, H., and Flörke, O.W. (1991) X-ray powder diffraction patterns and phase relationship of tridymite modifications. Zeitschrift für Kristallographie, 195, 31–48.

Grant, R. (1967) New data on tridymite. American Mineralogist, 52, 536–541.

Hoffmann, W. (1967) Gitterkonstanten und Raumgruppe von Tridymite bei 20 °C. Naturwissenschaften, 54, 114.

Hoffmann, W., and Laves, F. (1964) Zur Polytypie und Polytropie von Tridymit. Naturwissenschaften, 51, 335.

Kihara, K. (1977) An orthorhombic superstructure of tridymite existing between about 105 and 180 °C. Zeitschrift für Kristallographie, 146, 185–203.

——— (1978) Thermal change in unit-cell dimensions and a hexagonal structure of tridymite. Zeitschrift für Kristallographie, 148, 237–253.

Kihara, K., Matsumuto, T., and Imamura, M. (1986) High-order thermal motion tensor analyses of tridymite. Zeitschrift für Kristallographie, 177, 39–52.

Mosesman, M.A., and Pitzer, K.S. (1941) Thermodynamic properties of the crystalline forms of silica. Journal American Chemical Society, 63, 2348–2356.

Nukui, A., Nakazawa, H., and Akao, M. (1978) Thermal changes in monoclinic tridymite. American Mineralogist, 63, 1252–1259.

Press, W.H., Flannery, B.P., Teukolsky, S.A., and Vetterling, W.T. (1986) Numerical recipes, p. 289–293. Cambridge University Press, Cambridge, U.K.

Reid, A.M., Williams, R.J., and Takeda, H. (1974) Coexisting bronzite and clinobronzite and the thermal evolution of the Steinbach meteorite. Earth and Planetery Science Letters, 22, 67–74.

Shahid, K.A., and Glasser, F.P. (1970) Thermal properties of tridymite: 25 °C–300 °C. Journal of Thermal Analysis, 2, 181–190.

Smelik, E.A., and Reeber, R.R. (1990) A study of thermal behaviour of terrestrial tridymite by continuous X-ray diffraction. Physics and Chemistry of Minerals, 17, 197–206.

Tagai, T., Sadanaga, R., Takeuchi, Y., and Takeda, H. (1977) Twinning of tridymite from the Steinbach meteorite. Mineralogical Journal of Japan, 8, 382–398.

Thompson, A.B., and Wennemer, M. (1979) Heat capacities and inversions in tridymite, cristobalite and tridymite-cristobalite mixed phases. American Mineralogist, 64, 1018–1026.

Wennemer, M., and Thompson, A.B. (1984) Ambient temperature phase transitions in synthetic tridymite. Schweizerische mineralogische und petrographische Mitteilungen, 64, 355–368.

Wruck, B., Salje, E.K.H., and Grame-Barber, A. (1991) Kinetic rate laws derived from order parameter theory. IV: Kinetic of Al,Si disordering in Na-feldspars. Physics and Chemistry of Minerals, 17, 700–710.

Xiao, Y., Kirkpatrick, R.J., and Kim, Y.J. (1993) Structural phase transitions of tridymite: A ^{29}Si MAS NMR investigation. American Mineralogist, 78, 241–244.

Manuscript received November 30, 1993
Manuscript accepted March 24, 1994